Indian Journal of Chemistry
Vol. 59A, August 2020, pp. 1092-1099

Synthesis, characterization and photocatalytic dye degradation studies of novel defect pyrochlore, $KHf_{0.5}Te_{1.5}O_6$

M. Sudheera[a], G. Ravinder[b], G. Ravi[b], P. Venkataswamy[b], K. Vaishnavi[b], N. Chittibabu[c] & M. Vithal[b]*

[a]Department of Chemical Engineering, RVR and JC College of Engineering, Chowdavaram, Guntur - 522 019, India
[b]Department of Chemistry, University College of Science, Osmania University, Hyderabad - 500 007, India
[c]Department of Chemical Engineering, Andhra University, Visakhapatnam - 530 003, India
E-mail: mugavithal@gmail.com

Received 12 February 2020; revised and accepted 27 April 2020

In this study, $KHf_{0.5}Te_{1.5}O_6$ (KHTO) semiconductor has been synthesized by the solid-state method. The synthesized material is characterized using X-ray diffraction, Fourier transform infrared spectroscopy, UV-visible diffuse reflectance spectroscopy, field emission-scanning electron microscopy, energy dispersive spectroscopy, X-ray photoelectron spectroscopy and N_2 adsorption/desorption measurements. The material is found to be crystallized in a cubic lattice with the space group $Fd\bar{3}m$. The bandgap energy of the KHTO is 2.6 eV. The photocatalytic activity of KHTO has been investigated by measuring the degradation of methylene blue (MB) and methyl violet (MV) dyes under the visible light irradiation. The mechanistic dye degradation pathway of MB has been studied. The radical quenching experiments reveal that the short-lived species $O_2^{\bullet-}$, $OH^{\bullet}$, and h^+ actively participate in the degradation of MB and MV dyes. An additional terephthalic acid experiment has been carried out to establish the participation of $OH^{\bullet}$ radicals in the dye degradation. The stability and reusability of the KHTO catalyst are also studied.

Keywords: Powder XRD, Bandgap energy, Photocatalysis, Scavengers test, $OH^{\bullet}$ radicals

The investigation for new materials in the field of energy and environmental applications is of significant interest. Photocatalysis is one of the vital ecological claims in the water purification process because of its functional properties under solar light, which is an adequately available incessant resource. Hence, considerable investigations were carried out towards the development of efficient photocatalysts for energy and environmental applications[1-3]. However, most of the established photocatalysts are UV light active with bandgap energy above 3.0 eV[4-7]. The material with high bandgap energy restricts its photocatalytic ability in the visible region. Therefore, to attain an efficient photocatalyst that can work under the visible region is still a significant challenge to researchers.

In search of efficient visible-light-driven catalysts, we choose defect pyrochlores because of its large variety of properties that include structural flexibility, fast ionic conductivity, and photocatalytic behavior[8-13]. The general formula of the defect pyrochlore is AB_2O_6. Depending on the oxidation state of A and B cations, defect pyrochlores can be classified as $A^+B^{5+}B'^{6+}O_6$, $AB_{0.5}{}^{4+}B'^{6+}{}_{1.5}O_6$, and $AB^{3+}{}_{0.33}B'^{6+}{}_{1.67}O_6$. The defect pyrochlore structure is built by corner-sharing $BO_6/B'O_6$ octahedral units creating networks of hexagonal $BB'O_6$ tunnels, as shown in Fig. 1. The monovalent cation A is present in these tunnels. In defect pyrochlores, B cations and oxygen ions are present in *16d* (0.5, 0.5, 0.5) and *48f* (*x*, *0.125*, *0.125*) Wyckoff positions, respectively. The "A" ion occupies *8b* (0.375, 0.375, 0.375) or *16d* (0.5, 0.5, 0.5) or *32e* (x, x, x) sites depending on order/disorder in the "A" sublattice of AB_2O_6[8]. The A ions are easily exchangeable with other di, tri and tetravalent ions that lead to a variety of defect pyrochlore compositions with modified properties[14-18].

The literature on defect pyrochlores reveals that considerable research work on their photocatalytic activity has been carried out[8, 14-19]. However, the

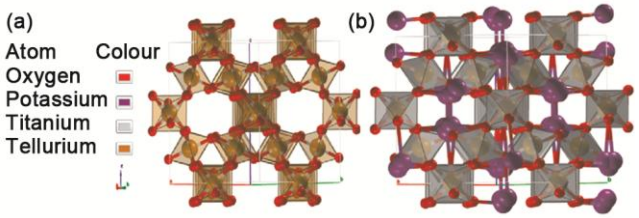

Fig. 1 — (a) Schematic for B_2O_6 octahedra network and (b) structure of $KHf_{0.5}Te_{1.5}O_6$ (KHTO).

photocatalytic activity of tellurium containing defect pyrochlores is less explored. Here, we report the synthesis, characterization, and photocatalytic studies of novel defect pyrochlore, $KHf_{0.5}Te_{1.5}O_6$.

Materials and Methods

Synthesis of $KHf_{0.5}Te_{1.5}O_6$ (KHTO)

The composition $KHf_{0.5}Te_{1.5}O_6$ is synthesized using the conventional solid-state method. Reagent grade K_2CO_3 (SD Fine, 99.99%), HfO_2 (Sigma Aldrich, 99.99%), and TeO_2 (Sigma Aldrich, 99.99%) chemicals were used as starting materials as received. The stoichiometric amounts of starting materials were thoroughly crushed in an agate mortar in the presence of spectral grade acetone and heated for 24 h at 550 °C in porcelain crucible in air. The resultant material is named as KHTO.

Characterization techniques

The powder X-ray diffraction (XRD) patterns were recorded using Rigaku miniflex 600 powder X-ray diffractometer (Cu-Kα, λ = 1.5406 Å) in the 2θ range of 10°-80° for phase confirmation. JASCO V650 UV-visible spectrophotometer was used for UV-visible diffuse reflectance spectra (DRS) measurements in the range of 200–900 nm. The reflectance standard used is $BaSO_4$. Field emission-scanning electron microscope (FESEM) analysis was performed using a Carl Zeiss model Ultra 55 electron instrument to analyze the morphology of the prepared sample and the composition of elements was obtained using energy dispersive spectroscopy (EDS). The Fourier transform infrared spectroscopy (FTIR) was performed in the form of KBr pellets in the wavenumber range 4000–350 cm^{-1} using JASCO IR-5300 spectrometer. X-ray photoelectron spectroscopy (XPS) analysis is performed on AMICUS/ESCA 3400 electron spectrometer using monochromatic Al-Kα radiation (1486.7 eV, 200W) as the excitation source at room temperature. The resulted binding energies are corrected by referencing the spectra to the C 1s peak at 284.6 eV. Nitrogen adsorption/desorption measurements are performed at 77 K with Micromeritics ASAP 2020 system. The surface area and pore size distribution of KHTO are estimated based on the BET and BJH methods, respectively.

Photocatalytic experiments

The photocatalytic efficiency of the KHTO was assessed by the photodegradation of methylene blue (MB) and methyl violet (MV) dyes using HEBER visible annular type photoreactor equipped with a 300 W tungsten lamp. The procedure is as follows: Aqueous MB/MV solution with (50 mL) an initial concentration of 1 x 10^{-5} M and 50 mg of KHTO catalyst were taken in a cylindrical-shaped glass reactor at room temperature. The resultant suspension was stirred in a dark chamber for 60 min to establish adsorption-desorption equilibrium before irradiation of light with continuous air bubbling to ensure a constant source of dissolved oxygen. At regular time intervals of 30 min, about 2-3 mL of the solution was collected and centrifuged to remove the KHTO particles. The change in the concentration of MB/MV was obtained by recording the absorbance at 664/580 nm using the JASCO V650 UV-visible spectrophotometer. The degradation amount of dyes was calculated from the equation

$$D = \left(\frac{C_{eq} - C}{C_{eq}} \right) \times 100\%$$

Here, D is the percentage of degradation, C_{eq} is the concentration of dye when adsorption-desorption equilibrium is achieved, and C is the concentration at time t.

Mechanistic studies of photocatalyst

The establishment and contribution of photogenerated species such as hydroxyl, superoxide radicals and holes, during photocatalysis in the degradation of MB dye, was studied by quenching experiments. Accordingly, tertiary butanol (TB), benzoquinone (BQ), and ammonium oxalate (AO) were used as quenchers for hydroxyl, superoxide radicals and holes, respectively[20-22]. About 50 mg of KHTO sample is dispersed in 50 mL of methyl violet dye solution containing 2 mL of 2 mM TB, BQ, and AO and placed separately in different tubes inside the photoreactor. Samples were allowed to attain adsorption-desorption equilibrium in the dark for about 60 min and then irradiated with visible light. During irradiation, 2-3 mL of sample was collected every 30 min, and absorbance was recorded. The formation of hydroxyl radicals during photocatalysis was also followed by the measurement of fluorescence intensity of 2-hydroxy terephthalic acid as reported[14, 23]. Typically, 50 mg of KHTO was suspended into 50 mL of a 0.02 M NaOH solution containing 3 mM terephthalic acid (TA). The suspension was stirred in the dark for 60 min. Then, 2-3 mL of the suspension was taken out at every

30 min time intervals, then filtered and recorded fluorescence spectra using Shimadzu RF-5301PC fluorescence spectrophotometer. The photogenerated $OH^{\bullet}$ species react with TA to form 2-hydroxy terephthalic acid (TAOH), which shows a characteristic fluorescence signal at 425 nm. The increase in the fluorescence intensity of TAOH was directly proportional to the concentration of photogenerated $OH^{\bullet}$ species. The excitation wavelength was fixed at 320 nm.

Results and Discussion

XRD and FTIR analysis

The defect pyrochlore KHTO is prepared by the solid-state method. Its powder XRD pattern is recorded to confirm the phase formation (Fig. 2). The resultant powder pattern is compared with the reported XRD pattern of $KTi_{0.5}Te_{1.5}O_6$ (JCPDF No. 84-1915). It is perceived that all the diffraction peaks of KHTO are consistent with the reported $KTi_{0.5}Te_{1.5}O_6$ and free from impurities. Hence, it is believed that KHTO is isomorphous with the $KTi_{0.5}Te_{1.5}O_6$ structure, and all the observed powder diffraction peaks can be indexed to a cubic lattice with $Fd\bar{3}m$ space group. The relatively high intensity of *d*-lines and low background indicate the good crystallinity of the KHTO. The structural refinement of KHTO is carried out by Rietveld method using Fullprof software. The initial lattice parameters of $KTi_{0.5}Te_{1.5}O_6$ are taken to refine the structural parameters of KHTO. The observed and calculated diffraction patterns of KHTO are given in Fig. 3 and the unit cell parameters of KHTO along with its crystallographic sites in Table 1. The composition KHTO is further characterized by recording its infrared spectrum. The FTIR spectrum of KHTO is presented in Fig. 4. The observed vibrational modes below 1000 cm^{-1} are characteristic of reported defect pyrochlores[24-25]. The vibrational band around 750 cm^{-1} can be attributed to Hf–O or Te–O stretching vibrations in the HfO_6/TeO_6 octahedra, and the band near 500 cm^{-1} is endorsed to the K-O stretching vibrational mode. The weak bands around 3500, 1600, and 1130 cm^{-1} can be attributed to O-H stretching vibrations of adsorbed atmospheric moisture due to its structural defects[16].

Table 1 — R factors, the unit cell parameters and Wyckoff positions of atoms in KHTO

$a = b = c = 10.1924$ Å, $R_{wp} = 12.56$, $R_{exp} = 8.83$ and $\chi^2 = 1.422$

Atom	Wyckoff position	*x*	*y*	*z*
K	*32e*	0.1046	0.1046	0.1046
Hf	*16d*	0.5	0.5	0.5
Te	*16d*	0.5	0.5	0.5
O	*48f*	0.4229	0.125	0.125

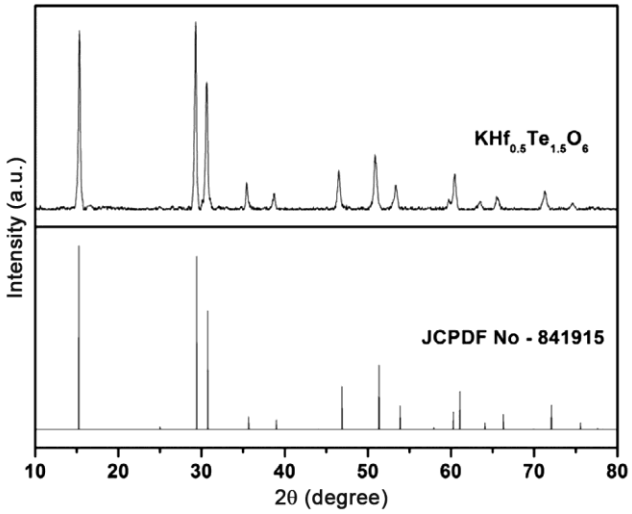

Fig. 2 — XRD pattern of $KHf_{0.5}Te_{1.5}O_6$ (KHTO).

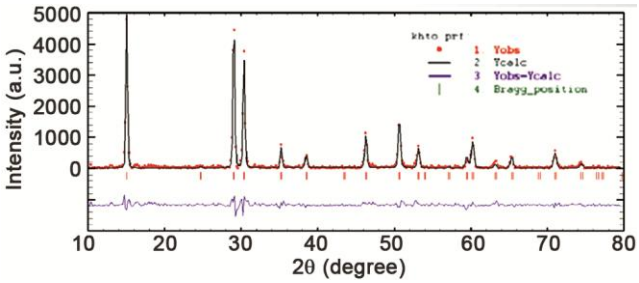

Fig. 3 — Observed and calculated patterns of $KH_{0.5}Te_{1.5}O_6$ (KHTO).

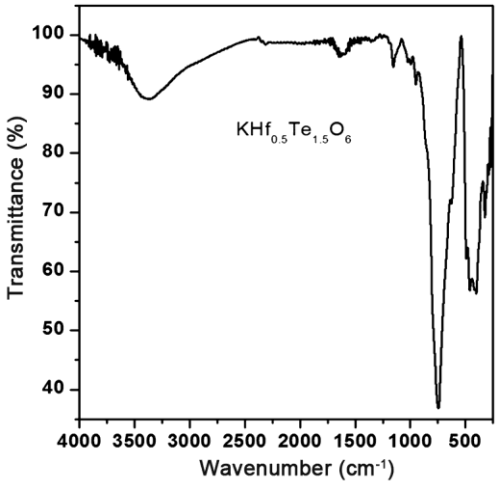

Fig. 4 — Fourier transform infrared spectrum $KHf_{0.5}Te_{1.5}O_6$ (KHTO).

UV-visible DRS, FESEM/EDS and XPS analysis

The optical absorbance of the KHTO is studied by UV-visible DRS technique. Fig. 5a shows the absorbance profile of KHTO. The absorption edge of KHTO is in the visible region and found to be at 585 nm. The bandgap energy (E_g) of the material KHTO is realized from the Kubelka-Munk plot[23] (KM vs. hν, where KM = $(Khν)^{1/2}$) (Fig. 5b). The bandgap energy of KHTO is found to be 2.6 eV.

The surface morphology and elemental composition of KHTO are obtained from FESEM/EDS measurements. As shown in Fig. 6a, the image of KHTO exhibits a well-defined agglomerate of hexagonal and cube-shaped particles. Further, the intensity ratio of K, Hf, Te, and O is found to be 1:0.5:1.5:6 confirming the composition as $KTi_{0.5}Te_{1.5}O_6$ (Fig. 6b). XPS measurement was used to characterize the surface chemical composition and chemical states of elements present in the KHTO sample. The XPS survey scan spectrum (Fig. 7a) of KHTO reveals the presence of K, O, Te, and Hf elements. The peaks observed at 530.2, 517.2, 292.6, and 284.8 eV can be ascribed to O 1s, Te 3d, K 2p, and Hf 4d, respectively. As shown in Fig. 7b, a broad peak centered at 295.2 eV is due to potassium ions in +1 oxidation state[26]. Two strong peaks at 578. 5 and 588.9 eV is attributed to Te $3d_{3/2}$ and Te $3d_{5/2}$, respectively, indicating the Te ions in 6+ oxidation state (Fig. 7c)[27]. Two characteristic peaks are observed at binding energies 213.2, and 224.1 eV correspond to Hf $4d_{5/2}$ and Hf $4d_{3/2}$, respectively (Fig. 7d). This result suggests that Hf is present in the KHTO sample as Hf^{4+}.[28] The O 1s peak is fairly broad and can be deconvoluted into three peaks with different binding energies: OI: 529.2, OII: 530.8 and OIII: 532.7 eV, corresponding to lattice oxygen, surface adsorbed oxygen and oxygen in the water/carbonate molecules, respectively (Fig. 7e)[7].

The textural characteristics of the as-prepared KHTO material are determined by the N_2 adsorption/desorption measurements. As shown in Fig. 8, the N_2 adsorption/desorption isotherm of KHTO corresponds to the type-IV curve with the H1 hysteresis loop (IUPAC classification), which is typical of the mesoporous nature of materials[29]. Fig. 8 inset shows the corresponding pore size distribution

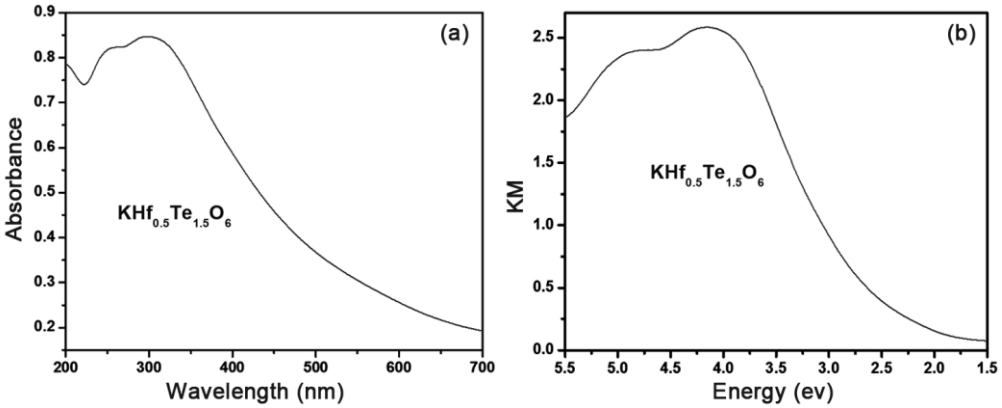

Fig. 5 — (a) UV-visible absorption spectrum and (b) derived KM plot of $KH_{0.5}Te_{1.5}O_6$ (KHTO).

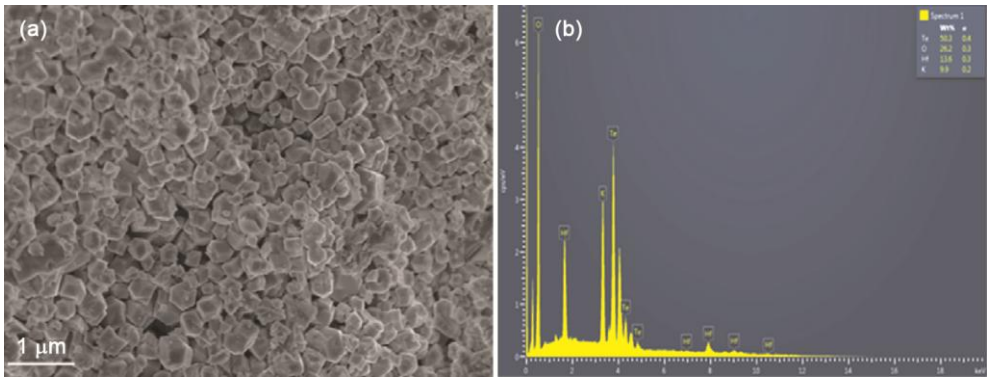

Fig. 6 — (a) FESEM image and (b) EDS profile of $KHf_{0.5}Te_{1.5}O_6$ (KHTO).

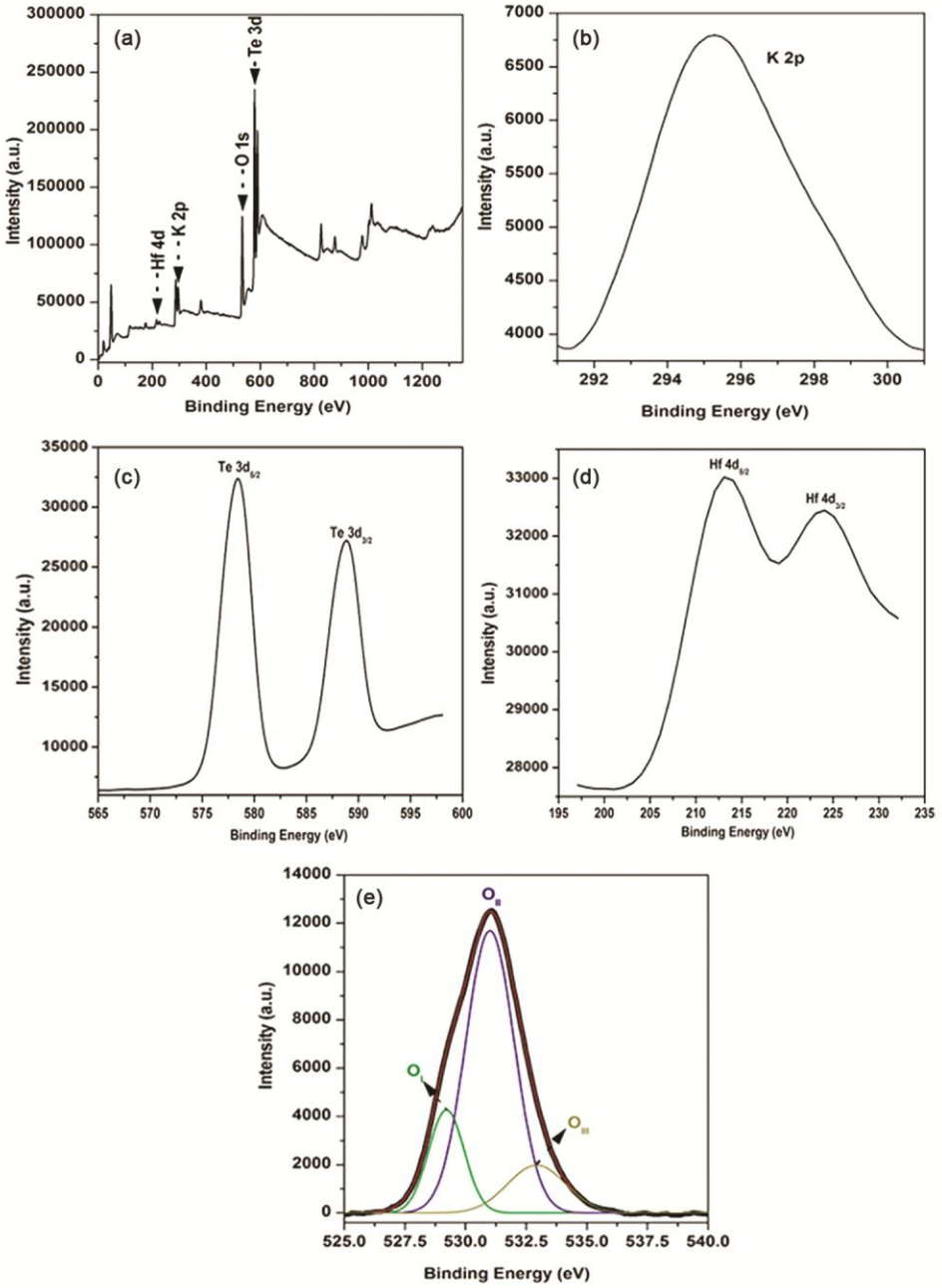

Fig. 7 — XPS spectra of $KHf_{0.5}Te_{1.5}O_6$ (KHTO): (a) wide survey spectrum, (b) K 2p, (c) Te 3d, (d) Hf 4d and (e) O 1s.

curve calculated by the BJH method. It is clear that the KHTO sample exhibits a multimodal distribution (between 8 to 25 nm) with the pore diameters of 8.9, 14.7, and 18.7 nm. The BET surface area and pore volume of the KHTO sample are 31.2 m^2 g^{-1} and 0.24 cm^3 g^{-1}, respectively.

Photocatalytic activity

The photocatalytic activity of KHTO is studied against the degradation of MB and MV dyes under visible light irradiation. Fig. 9 shows the variation in concentration of MB and MV dyes under the visible light irradiation up to 180 min for KHTO. During the dark reaction, about 6 and 10 % of MB and MV are adsorbed onto the surface of the KHTO, respectively. It is observed from Fig. 9 that the concentration of dyes decreased with the increase in irradiation time, indicating the degradation in presence of KHTO. The overall degradation

percentage of MB and MV in the presence of KHTO within 180 min of irradiation time was found to be 90% and 81%, respectively. It is known that the colored dyes undergo self-degradation (photolysis) to some extent in the presence of light irradiation. Hence, to determine the catalytic activity of KHTO, photolysis of MB and MV under identical experimental conditions is also carried out. The degradation of MB and MV without KHTO catalyst is found to 29% and 12%, respectively. Thus, the observed above 80% degradation for both dyes is significantly due to photocatalysis.

The photocatalytic dye degradation mechanism is complex due to the involvement of different radical species participating in the multistep degradation process. The main species involved in the dye degradation reaction are holes (h^+), hydroxyl radicals ($OH^\bullet$), and superoxide radicals ($O_2^{\bullet-}$). When the catalyst absorbs the light energy greater than its bandgap energy, the electron-hole pairs are produced. These photogenerated electron-hole pairs react with surface OH^- species and adsorbed oxygen from aqueous dye solution and produce oxidative species $OH^\bullet$ and $O_2^{\bullet-}$, respectively. Subsequently, these short-lived $OH^\bullet$ and $O_2^{\bullet-}$ species react with dye molecules and degrade them into CO_2 and water. Thus, the existence of oxidative species is essential for establishing the photocatalytic mechanism.

To investigate the generation and the participation of these oxidative species in the photodegradation of MB in the presence of KHTO, additional experiments like scavengers test and terephthalic acid (TA) experiments were carried out. Scavengers such as tertiary butanol (TB), ammonium oxalate (AO), and benzoquinone (BQ) are used for quenching the photogenerated $OH^\bullet$, h^+, and $O_2^{\bullet-}$ respectively (Fig. 10a). The percentage of degradation of MB after the addition of TB, AO, and BQ quenchers was found to be 61, 74 and 66% (it was 90% without TB, AO, and BQ separately), respectively. This confirms the active participation of h^+, $OH^\bullet$ and $O_2^{\bullet-}$ in the degradation of MB dye.

Further, an additional experiment was also carried out to endorse the generation of hydroxyl radicals during photocatalytic reactions using terephthalic acid (TA) as a probe. It is established that $OH^\bullet$ react with TA and gives 2-hydroxy terephthalic acid (TAOH). The TAOH emits a distinctive fluorescence peak at 425 nm with the excitation wavelength of 320 nm. The formation of TAOH is taken as an indication for the generation of $OH^\bullet$, radicals. Fig. 10b shows the fluorescence spectra of visible light irradiated KHTO suspension in 3 mM terephthalic acid (λ_{ex} = 320 nm) as a function time of irradiation. It is observed that, with continuous irradiation time, the intensity of fluorescence signals is increased progressively, representing the escalation in the concentration of $OH^\bullet$ radicals during the photocatalytic reaction. Based on these additional experiments, the expected dye degradation mechanism is given below.

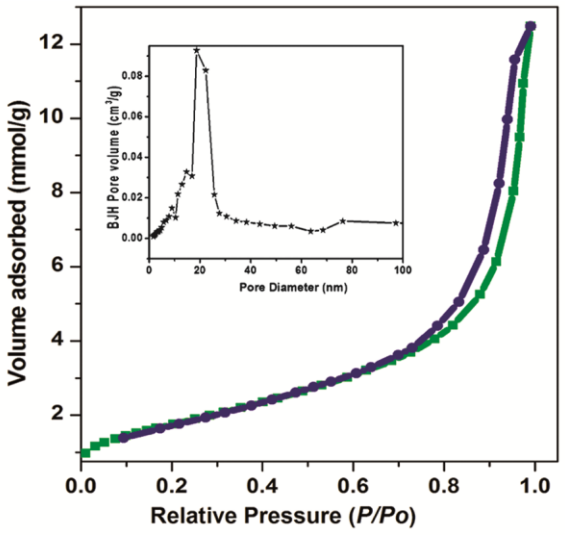

Fig. 8 — N_2 adsorption/desorption isotherm of $KHf_{0.5}Te_{1.5}O_6$ (KHTO) (BJH pore size distribution curve is shown in the inset).

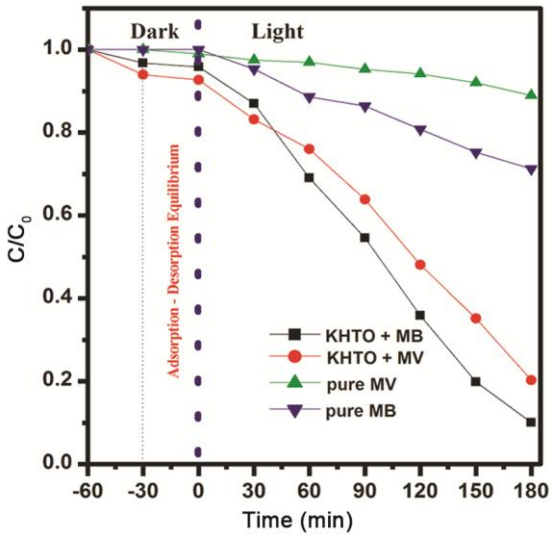

Fig. 9 — The photodegradation curves of MB and MV dyes within 180 min of visible light irradiation over $KHf_{0.5}Te_{1.5}O_6$ (KHTO).

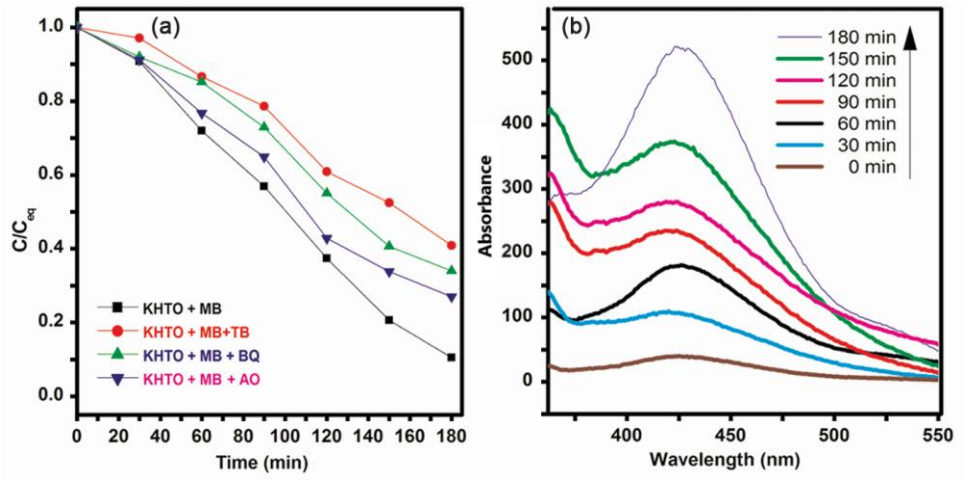

Fig. 10 — (a) Photodegradation of MB using $KHf_{0.5}Te_{1.5}O_6$ (KHTO) with and without tertiary butanol, ammonium oxalate and benzoquinone and (b) Fluorescence spectra of visible light irradiated $KHf_{0.5}Te_{1.5}O_6$ (KHTO) suspensions in 3 mM terephthalic acid (λ_{ex}=320 nm).

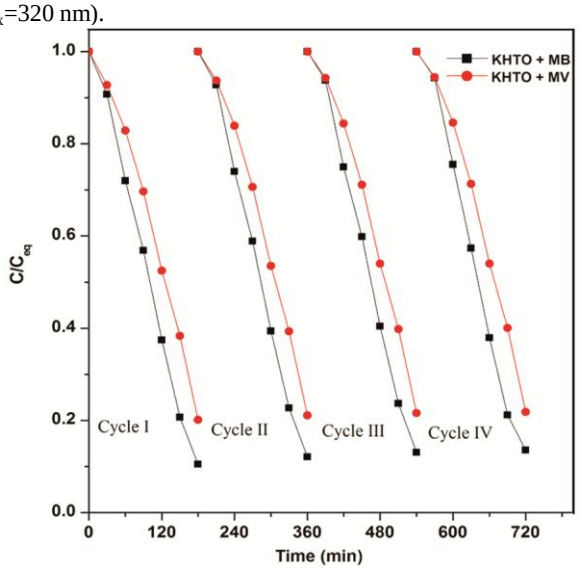

Fig. 11 — Cycling runs in photodegradation of MB and MV dyes in the presence of $KH_{0.5}Te_{1.5}O_6$ (KHTO).

$$KHTO + h\nu \rightarrow e^{-}_{CB} + h^{+}_{VB}$$
$$H_2O + h^{+}_{VB} \rightarrow OH^{\bullet} + H^{+}$$
$$O_2 + e^{-}_{CB} \rightarrow O_2^{\bullet -}$$
$$O_2^{\bullet -} + H^{+} \rightarrow HO_2^{\bullet}$$
$$2HO_2^{\bullet} \rightarrow H_2O_2 + O_2$$
$$H_2O_2 \rightarrow 2OH^{\bullet}$$
$$HO_2^{\bullet} \text{ or } O_2^{\bullet -} \text{ or } OH^{\bullet} + MB \rightarrow Byproducts$$

The stability and reusability of KHTO are essential concerns for practical applications in the catalysis field. The cyclic runs of MB and MV photodegradation experiments in the presence of KHTO are carried out to test the catalyst stability and reusability. After each cycle of photocatalytic experiment, the KHTO catalyst is separated, washed with distilled water to remove the adsorbed dye molecules, and reused for the next cyclic photocatalytic reaction with a fresh batch of dye solutions. Fig. 11 shows the variation in concentration of MB and MV with irradiation time for four cycles. It is noticed that the photocatalytic dye degradation percentage in the presence of KHTO is almost the same for all four cyclic runs. Thus, it can be concluded that the photocatalyst KHTO is stable and reusable at least up to four times.

Conclusions

The photocatalyst $KHf_{0.5}Te_{1.5}O_6$ is prepared through a solid-state method at 550 °C for 24 h. The Rietveld refinement results confirm the cubic structure of KHTO with $Fd\bar{3}m$ space group. The pore volume and BET surface area of the KHTO sample is 0.24 $cm^3\ g^{-1}$ and 31.2 $m^2\ g^{-1}$, respectively. The bandgap energy of the KHTO is deduced from the KM plot and found to be 2.6 eV. The EDS and XPS results support the elemental composition of KHTO as $KHf_{0.5}Te_{1.5}O_6$. The material has exhibited photoactivity against the degradation of MB and MV dyes under visible light irradiation. The degradation percentage of MB and MV in the presence of KHTO within 180 min of irradiation is found to be 90% and 81%, respectively. The contribution of h^+, $O_2^{\bullet -}$ and $OH^{\bullet}$ during photocatalytic MB dye degradation is confirmed from quenching experiments. Further, the generation of $OH^{\bullet}$ radicals during photocatalysis is

also established from the terephthalic acid experiment. Finally, photocatalyst KHTO is stable and reusable for at least up to four cycles.

Acknowledgment

MS gratefully acknowledges the funding agency, University Grant Commission (UGC), India, for providing financial support, in the form of SERO/UGC. The Science and Engineering Research Board (SERB) (Grant No. EMR/2016/001533), Department of Science and Technology (DST), India, is acknowledged for its financial support. MV thanks to UGC, New Delhi, for the award of BSR fellowship [F.18–1/2011(BSR)].

References

1 Zhang G, Liu G, Wang L & Irvine J T S, *Chem Soc Rev*, 45 (2016) 5951.
2 Afroz K, Moniruddin Md, Bakranov N, Kudaibergenov S & Nuraje N, *J Mater Chem A*, 6 (2018) 21696.
3 Yang N, Li G, Yang X, Wang W & Zhang W F, *Dalton Trans*, 40 (2011) 3459.
4 Hoffmann M R, Martin S T, Choi W & Bahnemann D W, *Photocatal Chem Rev*, 95 (1995) 69.
5 Linsebigler A L, Lu G & Yates J T, *Chem Rev*, 95 (1995) 735.
6 Kudo A & Kato H, *Chem Lett*, 5 (1997) 421.
7 Sreenu K, Venkataswamy P, Ravi G, Reddy C S, Reddy B J & Vithal M, *Z Anorg Allg Chem*, 645 (2019) 529.
8 Subramanian M A, Aravamudan G & Rao G V S, *Pro Solid State Chem*, 15 (1983) 55.
9 Goodenough J B, Hong H Y P & Kafalas J A, *Mater Res Bull*, 11 (1976) 203.
10 Kako T, Kikugawa N, Ye J & *Catal Today*, 131 (2008) 197.
11 Ishihara T, Seok Baik N, Ono N, Nishiguchi H & Takita Y, *J Photochem Photobiol A*, 167 (2004) 149.
12 Ikeda S, Fubuki M, Takahara Y K & Matsumura M, *Appl Catal A*, 300 (2006) 186.
13 Zhang G, Jiang W & Yu S, *Mater Res Bull*, 45 (2010) 1741.
14 Guje R, Ravi G, Palla S, Rao K N & Vithal M, *Mater Sci Eng B*, 198 (2015) 1.
15 Uma S, Singh J & Thakral V, *Inorg Chem*, 48 (2009) 11624.
16 Guje R, Ravi G, Kadari R, Sreenu K, Sudhakar Reddy Ch, Malathi M, Velchuri R, & Vithal M, *Indian J Chem*, 55A (2016) 1174.
17 Ravi G, Kumar K S, Guje R, Sreenu K, Prasad G & Vithal M, *J Solid State Chem*, 233 (2016) 342.
18 Guje R, Ravi G, Reddy J R, Veldurthi N K, Sreenu K & Vithal M, *Photochem Photobiol*, 92 (2016) 223.
19 Jitta R R, Ravi G, Veldurthi N K, Guje R & Vithal M, *J Chem Technol Biotechnol*, 90 (2015) 1937.
20 Jitta R R, Guje R, Veldurthi N K, Prathapuram S, Velchuri R & Muga V, *J Alloys Compd*, 618 (2015) 815.
21 Zhang N, Zhang Y, Yang M Q, Tang Z R & Xu Y J, *J Catal*, 299 (2013) 210.
22 Xu Y S & Zhang W D, *Dalton Trans*, 42 (2013) 1094.
23 Reddy J R, Veldurthi N K, Palla S, Ravi G, Guje R & Vithal M, *J Chem Technol Biotechnol*, 89 (2013) 1833.
24 Maczka M, Knyazev A V, Kuznetsov N Y, Ptaka M & Macalik L, *J Raman Spectrosc*, 42 (2011) 529.
25 Knyazev A V, Maczka M & Kuznetsova N Y, *Thermochim Acta*, 506 (2010) 20.
26 Venkataswamy P, Sudhakar Reddy Ch, Ravi G, Sadanandam G, Veldurthi N K & Vithal M, *Electron Mater Lett*, 14 (2018) 446.
27 Sathiya M, Ramesha K, Rousse G, Foix D, Gonbeau D, Guruprakash K, Prakash A S, Doublet M L & Tarascon J M, *Chem Commun*, 49 (2013) 11376.
28 Engelhard M, Herman J, Wallace R & Baer D, *Surf Sci Spectra*, 18 (2011) 46.
29 Huang S, Zhao Y, Hu X, Liu D, Wang X & Su Y, *J Nanopart Res*, 20 (2018) 281 (1-13).